Supporting Information

Zhou et al. 10.1073/pnas.1321926111

SI Text

Optics of Director Patterns in the Wake of Moving Bacterium. We numerically simulated the optical patterns observed under the polarizing microscope, using the standard Berreman 4 × 4 matrix method (1). We model the director field distorted by the flagella as follows:

$$n_y(x,y,z) = \sin\varphi_0 \sin(-kx)(1-\beta|z-z_0|)\exp\left(-\frac{|y-y_0|}{\lambda}\right),$$

$$n_z(x,y,z) = -\sin\varphi_0 \cos(-kx)(1-\beta|z-z_0|)\exp\left(-\frac{|y-y_0|}{\lambda}\right),$$

$$n_x(x,y,z) = \sqrt{1-n_y^2-n_z^2},$$

where $(x,y_0,z_0) = (x, r_0\cos(-kx), r_0\sin(-kx))$ defines the position of left-handed helical flagella along the x axis and centered at (0,0) of the y–z plane. By its rotation, director $\hat{\mathbf{n}}$ deviates from $\hat{\mathbf{n}}_0 = (1,0,0)$ by the angle $\varphi_0 = 10^\circ$ at the flagella and linearly decays in the z direction with the rates $\beta = \left(z_0+\frac{h}{2}\right)^{-1}$ (for $z<z_0$) and $\left(\frac{h}{2}-z_0\right)^{-1}$ (for $z\geq z_0$), and exponentially decays in the y direction with a characteristic decay length $\lambda = 1$ μm; $r_0 = 0.5$ μm is the rotation radius of flagella, $k = 2\pi P^{-1}$, and $P = 2$ μm is the helical pitch of the flagella. Using this model, we display in Fig. S1 the textures for different analyzer orientations in the area corresponding to four periods of the director pattern along the x direction and to 3λ along the y direction.

Optics of Director Patterns Distorted by Flows Produced by Individual Bacterium. Fig. 1*A* shows that the regions under and above a moving bacterium have a different optical density. Fig. S2 shows a clear manifestation of this effect for a bacterium that is pinned or does not swim (but is otherwise active and has rotating flagella), apparently because it is close to the stage of division into two bacteria and has two sets of flagella. For this bacterium, the optical density pattern resembles a butterfly (Fig. S2*A*) in which the director distortions propagate over tens of micrometers. PolScope image of the director field indicates that the director forms a tilted pattern in the shape of the letter X (Fig. S2*B*). The effect can be explained by the flow-induced reorientation of the director, schematically shown in Fig. S2*C* (see also Fig. 3*I*). Optical simulations based on the Berreman matrices show that these director distortions results in the butterfly pattern when the sample is observed between two polarizers (Fig. S2 *D*–*F*). Analytical calculation with the Jones matrix method shows that the field of light passing through a polarizer, a sample with retardance Γ oriented at φ, and an analyzer at φ_{AP} follows

$$\begin{bmatrix} E_a \\ 0 \end{bmatrix} = \frac{1}{\sqrt{2}}\begin{bmatrix} 1 & 0 \\ 0 & 0 \end{bmatrix}\begin{bmatrix} \cos\varphi_{AP} & \sin\varphi_{AP} \\ -\sin\varphi_{AP} & \cos\varphi_{AP} \end{bmatrix}\begin{bmatrix} \cos\varphi & -\sin\varphi \\ \sin\varphi & \cos\varphi \end{bmatrix}$$
$$\begin{bmatrix} e^{-i\Gamma/2} & 0 \\ 0 & e^{i\Gamma/2} \end{bmatrix}\begin{bmatrix} \cos\varphi & \sin\varphi \\ -\sin\varphi & \cos\varphi \end{bmatrix}\begin{bmatrix} 1 \\ 0 \end{bmatrix},$$

thus intensity at the analyzer

$$I_a = \frac{1}{2}\cos^2(\varphi_{AP}-\varphi)\cos^2\varphi + \sin^2(\varphi_{AP}-\varphi)\sin^2\varphi - \frac{1}{4}\sin 2(\varphi_{AP}-\varphi)\sin 2\varphi\cos\Gamma.$$

For $\Gamma = -1.15$ ($h = 5$ μm, $\Delta n = -0.02$, wavelength of the light 546 nm) as in our samples, I_a has minimum values at $\varphi_{AP} \approx 90^\circ + \frac{1}{2}\varphi$ when $\varphi < 25^\circ$. This confirms the experimental and optical simulation texture of "butterfly"-shaped director field (Fig. S2 *A*, *D*–*F*). For a moving bacterium, the effect is qualitatively similar, with the difference that the propulsion enhances the front two "wings" of the butterfly and weakens the rear two wings; as a result, the regions below and above the bacterium's head have different brightness (Fig. 1 *A* and *C*).

Besides the two coaxial streams, the bacterium also creates velocity fields associated with rotations of its body and its flagella (in opposite directions, Fig. S3 *A* and *B*). These rotations cause director reorientations that lack the mirror symmetry with respect to the plane passing through the long axis of the bacterium (Fig. S3*C*); these deformations would further complicate the director pattern in the close vicinity of a moving bacterium. These effects will be explored in detail in the future.

The director distortions would be created by a moving bacterium when the viscous torque overcomes the elastic one, which is equivalent to the requirement that the Ericksen number of the problem is larger than 1. For a rotating bacterium in a cell of thickness h, the Ericksen number (2) is $Er = \eta f r h/K$, where η is an effective viscosity, f is the frequency of bacterium head rotation, and r is the bacterium radius. For typical values of parameters in our problem, $K = 10$ pN, $\eta = 10$ kg/(m·s), $f = 2$ Hz, $r = 0.4$ μm, $h = 20$ μm, this requirement is easily satisfied, as $Er = 16$. As already discussed in the main text, the shear flows produced by the bacteria can also cause a decrease in the degree of orientational order, which corresponds to Deborah numbers close to 1 or larger.

Pattern Formation in the Director Dynamics: One-Dimensional Theory of Living Liquid Crystals. Let θ and ϕ be corresponding angles between the nematic director and bacteria with respect to the x axis. All of the quantities are averaged with respect to the thickness of the sample. For simplicity we focus on the one-dimensional situation (all quantities depend only on the x coordinate). We postulate the following equations of motion following from the fact that the nematic tends to align bacteria, and the bacteria tend to rotate the nematic director from that direction:

$$\eta\partial_t\theta = \frac{U}{2}\sin(2(\phi-\theta)) + K\frac{\partial^2\theta}{\partial x^2} - \varepsilon\sin(2\theta), \qquad \textbf{[S1]}$$

$$\eta\partial_t\phi = -\frac{A}{2}\sin(2(\phi-\theta)) + \mu\frac{\partial^2\phi}{\partial x^2}. \qquad \textbf{[S2]}$$

Here $U = cu_0 < 0$ is the averaged bacterial torque imposed on the director, c is the concentration of bacteria, $u_0 < 0$ is the bacteria hydrodynamic dipole moment, K is the liquid crystal elastic constant, A is the rate of alignment of bacteria by the liquid crystal, and μ is the effective bacterial diffusion (we assume in the following that $\mu >> K$ due to self-propulsion), and $\eta > 0$ is the rotational friction coefficient. The last term in Eq. **S1** describes an externally applied aligning (when $\varepsilon > 0$) or disorienting (when $\varepsilon < 0$) field that acts on the nematic. In a simplified one-dimensional model, this term can be qualitatively considered

as the surface anchoring; for $\varepsilon = 0$, all director orientations in the plane of the sample are degenerate.

Eqs. **S1** and **S2** display surprisingly rich dynamics. Consider first the case $\varepsilon = 0$ (no externally imposed aligning field). Examine the stability of a fully coaxial case, $\theta = \phi$. We seek the solution to linearized Eqs. **S1** and **S2** near $\theta = \phi$ in the form θ, $\phi \sim \exp(ikx + \lambda t)$. Here k, λ are the modulation wavenumber and instability growth rate, respectively. Simple stability analysis shows that the system exhibits a long-wavelength instability. The growth rate λ for small k is of the form

$$\lambda(k) = -\frac{AK + \mu U}{\eta(A + U)}k^2 + O(k^4). \qquad \textbf{[S3]}$$

Because the hydrodynamic dipole $U < 0$, then $\lambda > 0$ if $A > -U$ and $|U| > K\,A/\mu$. This instability leads to a rather nontrivial pattern formation. Further, we examine Eqs. **S1** and **S2** numerically, with and without surface anchoring. The equations show very rich spatiotemporal dynamics as shown in Fig. S4. If the externally imposed alignment is strong, no pattern appears and the fully aligned state of nematic and bacteria $\phi = \theta = 0$ is stable. Reduction of the strength ε of this externally imposed alignment (or, equivalently, increase of the bacterial activity torque U) leads to the onset of stripe pattern as shown in the space–time diagram (Fig. S4*A*). This regular stripe pattern seems to be stable (or, at least, very long-lived) only very close to the onset of instability. Further reduction of ε leads to a gradual instability of the stripes via side undulations and the onset of a spatiotemporal intermittency (Fig. S4*B*). In this case we observe patches of regular stripes mediated by randomly oriented domains, similar to that what we see in experiment for high concentration of bacteria. Finally, at $\varepsilon = 0$, we have randomly moving and oscillating domains with no preferred orientation (Fig. S4*C*). This case likely corresponds to the behavior in sessile drop where in-plane orientation is degenerate (Fig. S5*A*).

1. Yeh P, Gu C (1999) *Optics of Liquid Crystal Displays* (Wiley, New York).

2. Kleman M, Lavrentovich OD (2003) *Soft Matter Physics: An Introduction* (Springer, New York), p 638.

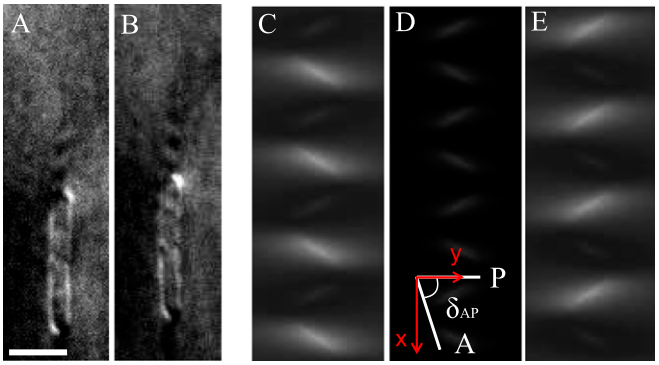

Fig. S1. Light intensity pattern for a linearly polarized light passing through the twisted director configuration as described in *SI Text, Optics of Director Patterns in the Wake of Moving Bacterium*. (*A* and *B*) Polarizing microscopy textures of oblique black and white regions in the wake area of swimming bacteria. (*C*–*E*) Optical simulation of director textures deformed by the helicoidal flagella viewed between two linear polarizers making a different angle δ_{AP}:=80° (*C*), 90° (*D*), and 100° (*E*). Scale bar, 5 μm.

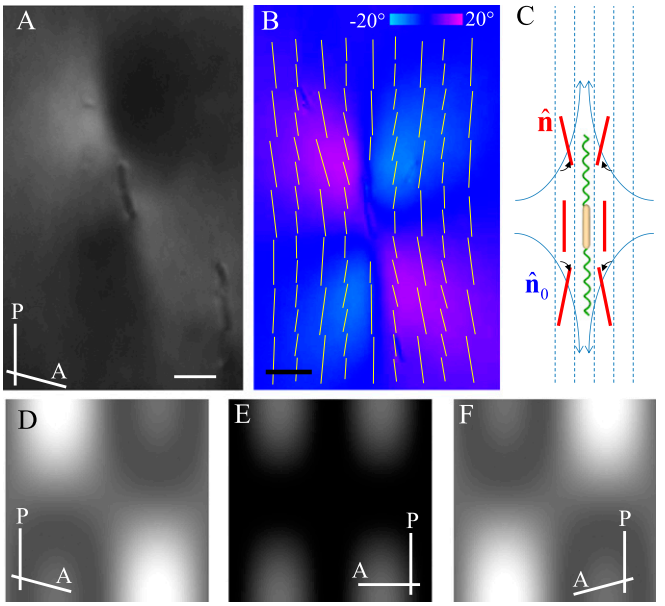

Fig. S2. Director distortions around an immobile bacterium. (*A*) Optical polarizing microscopy texture with de-crossed polarizers shows a butterfly pattern. (*B*) PolScope texture maps director pattern (yellow lines) resembling the letter X; color scale is proportional to the angle that the local director makes with the long axis of the image. (*C*) Schematic representation showing how the director (red bar) deviates from $\hat{\mathbf{n}}_0=(1,0,0)$ (blue dashed lines) due to the flow (blue arcs with arrows) induced by nonswimming two-tail bacterium. (*D–F*) Optical simulation of the director pattern in *B* shows the butterfly pattern in the intensity map when the two polarizers are crossed at different angles (*A* and *B*). Scale bar, 5 μm (*A*), 10 μm (*B*).

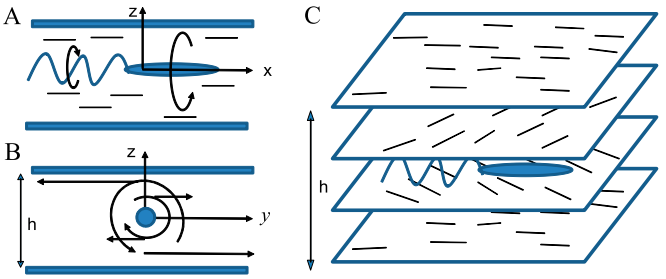

Fig. S3. Chiral symmetry breaking of the living liquid crystal (LLC) director pattern caused by a rotating bacterium. (*A* and *B*). Schematics of the flows generated by the rotating bacterium. (*C*) Scheme of the director twist along the vertical *z* axis.

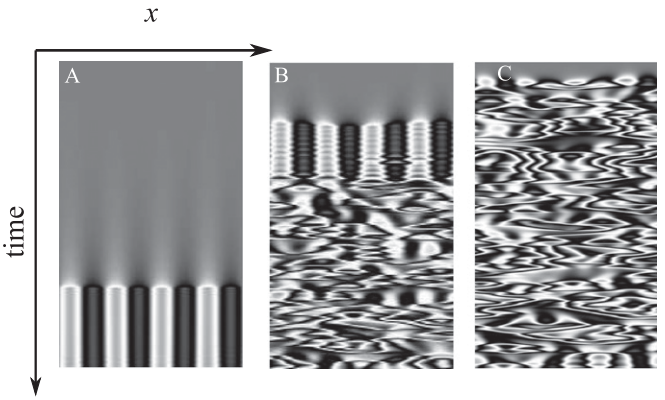

Fig. S4. Space–time diagrams obtained by numerical solution of Eqs. **S1** and **S2**. Gray-scale images show values of $\zeta=\sin(2(\phi-\theta))$, white corresponds to $\zeta=1$, and black to $\zeta=-1$. Parameters are $U=-0.3$, $K=1$, $A=1$, $\mu=10$, $\eta=1$, and for three values of the surface anchoring $\varepsilon=0.05$ (*A*), 0.04 (*B*), and 0 (*C*). Domain of integration is 100 units, and time of integration is 2,000 units of time. Integration is performed in periodic boundary conditions; initial condition was small noise around $\phi=\theta=0$ state.

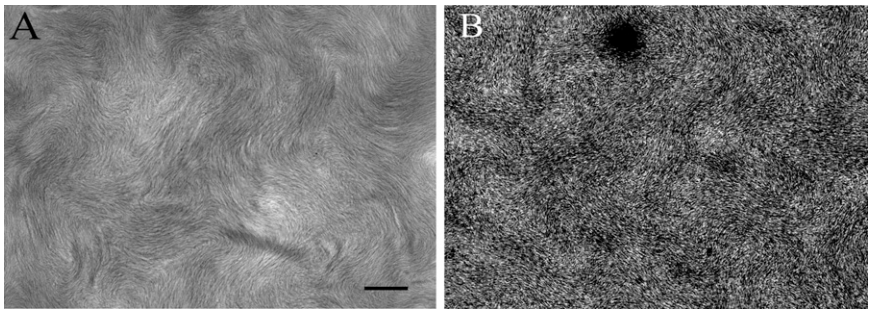

Fig. S5. Comparison of collective motion in the LLC (*A*) and in the Newtonian liquid (*B*). (*A*) Collective motion in the LLC, pattern of bacterial and nematic director orientation shows multiple $\pm 1/2$ defect pairs (the same as Fig. 3). Local, almost-perfect parallel orientation of bacteria is manifested by fine stripe texture. (*B*) Snapshot of collective motion in water for similar concentration of bacteria. Unlike the texture *A*, no fine stripe texture corresponding to local parallel alignment of bacteria can be identified in *B*. Scale bar, 30 μm for both images.

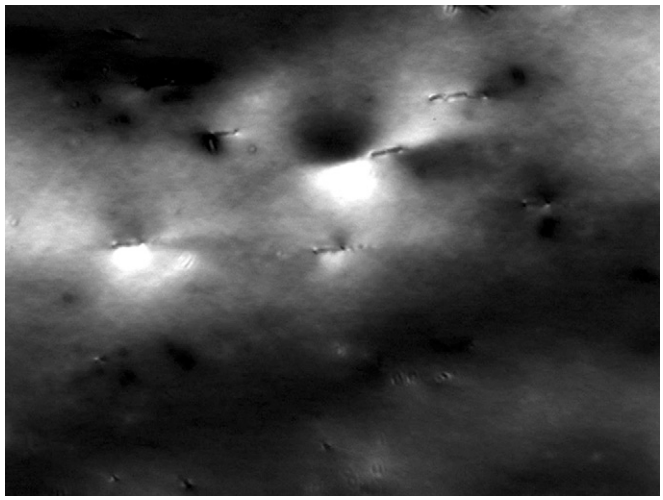

Movie S1. Distortions of the nematic director caused by swimming bacteria as observed under an optical microscope with slightly de-crossed polarizers. Flagella rotation generates a traveling wave pattern behind the bacteria. The video is recorded at 100 frames/s rate and played back at 25 frames/s (Fig. 1*A*).

Movie S1

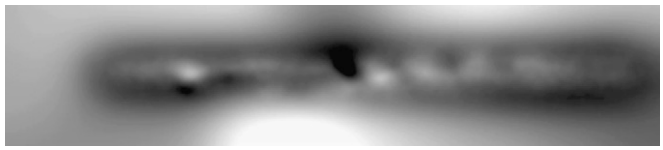

Movie S2. Distortions of the nematic director caused by rotating flagella in the comoving reference frame. Contrast is enhanced for the purpose of better visualization. The video is recorded at 100 frames/s rate and played back at 25 frames/s (Fig. 1*C*).

Movie S2

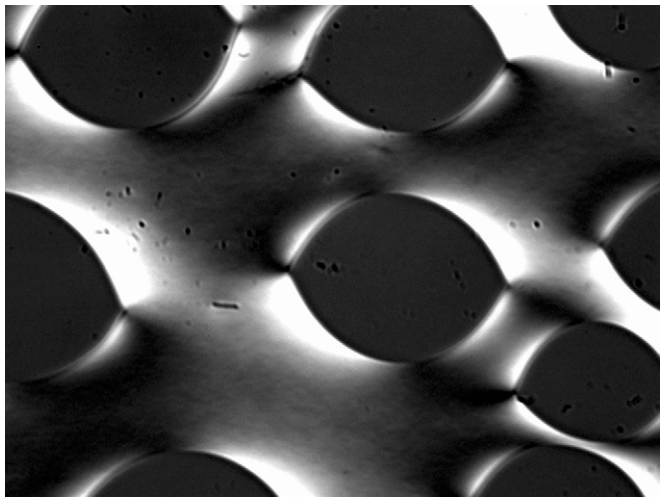

Movie S3. Motion of bacteria around isotropic tactoids (black elongated islands of isotropic phase). The video is recorded and played back at 25 frames/s (Fig. 1*E*).

Movie S3

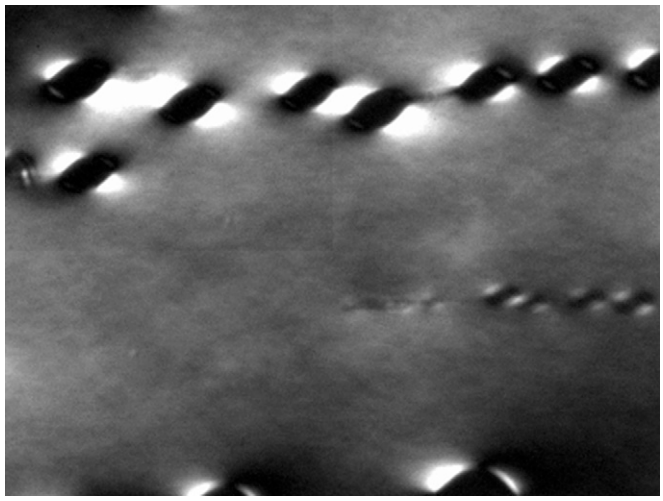

Movie S4. Swimming bacterium leaves a trace of isotropic tactoids. The video is recorded at 50 frames/s rate and played back at 25 frames/s (Fig. 1*F*).

Movie S4

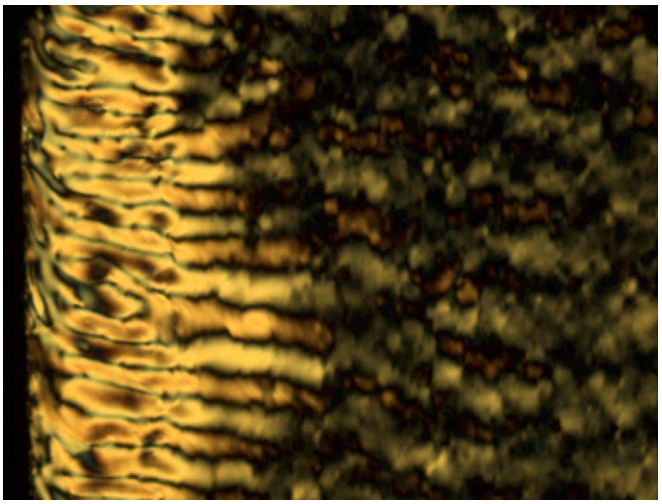

Movie S5. Formation of a stripe pattern perpendicular to the rubbing direction in the LLC sample of thickness $h = 20$ μm for low concentration of bacteria, $c \sim 0.9 \times 10^9$ cells/cm^3. The video is acquired under the optical microscope with crossed polarizers. Oxygen permeates from the left side. The video is recorded at 0.3 frames/s and played back at 30 frames/s (Fig. 2*E*).

Movie S5

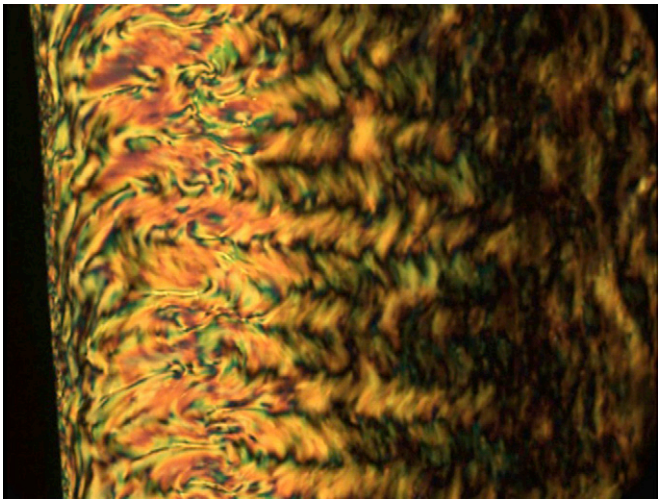

Movie S6. Formation of a stripe pattern with disclinations in the LCC sample ($h = 50$ μm) for high concentration of bacteria, $c \sim 1.6 \times 10^9$ cells/cm^3. During the video recording, the polarizer was removed and placed back two times. The video is recorded at 0.3 frames/s and played back at 30 frames/s (Fig. 2*F*).

Movie S6

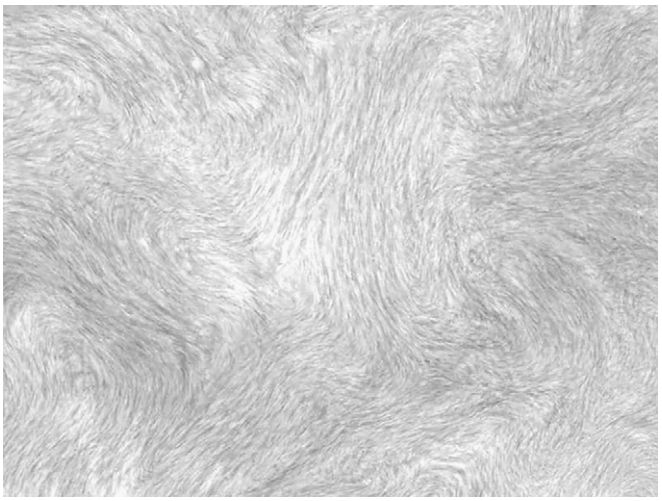

Movie S7. Dynamics of the LLC in sessile drop. The video is recorded and played back at 30 frames/s rate (Fig. 3*A*).

Movie S7